

RESEARCH ARTICLE

Transport Phenomena and Fluid Mechanics

Accelerating charging dynamics using self-driven optimizing porous structures

Pan Huang¹ | Haolan Tao^{1,2}  | Honglai Liu^{1,2} | Cheng Lian^{1,2} 

¹State Key Laboratory of Chemical Engineering, Shanghai Engineering Research Center of Hierarchical Nanomaterials, School of Chemical Engineering, East China University of Science and Technology, Shanghai, China

²School of Chemistry and Molecular Engineering, East China University of Science and Technology, Shanghai, China

Correspondence

Haolan Tao and Cheng Lian, State Key Laboratory of Chemical Engineering, Shanghai Engineering Research Center of Hierarchical Nanomaterials, School of Chemical Engineering, East China University of Science and Technology, Shanghai 200237, China.
Email: haolan_tao@ecust.edu.cn and lian Cheng@ecust.edu.cn

Funding information

the Fundamental Research Funds for the Central Universities, Grant/Award Number: 2022ZFJH004; the National Key R&D Program of China, Grant/Award Number: 2022YFA1503501; the National Natural Science Foundation of China, Grant/Award Numbers: 22078088, 22278127; the Shanghai Rising-Star Program, Grant/Award Number: 21QA1401900; Jiangsu Engineering Laboratory of New Materials for Sewage Treatment and Recycling

Abstract

Relating the complex structures of electrodes to their charging dynamics is crucial for optimizing supercapacitors, which remains an experimental and theoretical challenge. Here, we construct a pore network model (PNM) that can be downward-transformed into a well-known transmission-line model and a stack-electrode model to describe the disordered porous structure of carbon-based electrodes. A mathematical expression is derived using an equivalent circuit model of the PNM to quantify the relaxation times of the potential and concentration. The expression is then verified using numerical solutions based on the simplified Poisson–Nernst–Planck equations and experimental data. The structure of the PNM for experimental verification is directly extracted from a porous electrode reconstructed using a scanning electron microscopic image. A self-driven optimization framework is proposed by coupling the derived expression with a genetic algorithm to generate an optimal porous structure that can be used to investigate the changing dynamics of the electrode. Our framework provides a general image–structure–performance optimization platform for understanding and accelerating charging dynamics in porous electrodes.

KEYWORDS

charging dynamics, pore network model, porous electrode, relaxation time, structure optimization

1 | INTRODUCTION

Supercapacitors have attracted tremendous attention because of their high power density, excellent stability, and long cycling life compared with batteries; given these characteristics, these devices show great potential for use in portable electronics, green grids, and hybrid vehicles.^{1–3} Many porous carbon-based materials have been employed as electrodes in commercial supercapacitors owing to their low cost, convenient preparation, and large specific surface area.⁴ However, the relationship between the disordered microscopic structure of porous carbon-based electrodes and the charging dynamics of macroscopic supercapacitors is poorly understood, rendering the rational design of supercapacitors with higher performance difficult.^{1,5} The relaxation time τ is a physical quantity that is widely used to evaluate the

charging dynamics and represents the time scale at which the charge, potential, or concentration reaches equilibrium.^{5–10} Naturally, a shorter τ suggests increased charging efficiency. In general, the charging process of supercapacitors can be described by two types of τ ^{5,11,12}: the relaxation time of the potential τ_ϕ and the relaxation time of the concentration τ_c . τ_ϕ and τ_c represent the time scales at which the charging process is controlled by electric double layer (EDL) formation and ionic diffusion from the bulk to pores, respectively.

Currently, different methods exist for investigating the charging dynamics in porous electrodes: experiments,^{13,14} molecular dynamics (MD) simulations,^{15,16} and continuum modeling^{17,18}; these methods can elucidate the buildup of EDLs at the electrode/electrolyte interface and the charging mechanisms in a few nanopores as well as in disordered carbon materials. Song and Bazant¹⁹ developed a mathematical

framework to calculate the diffusion time by analyzing the electrochemical impedance spectra and inferring the microstructural statistics of random heterogeneous materials. Several porous electrode models have been proposed for studying ion transport and calculating τ_ϕ and τ_c . The validity of the transmission-line (TL) model pioneered by De Levie²⁰ for characterizing charging dynamics has been confirmed by many relevant studies.^{21–23} For example, using direct numerical calculations of the Poisson–Nernst–Planck (PNP) equations and TL theory, Gupta et al.²² studied the charging dynamics of overlapping double layers in a cylindrical nanopore and derived an expression for τ_ϕ . Janssen²⁴ extended the TL model for charging an electrolyte-filled nanopore of finite length to discuss the intimate relationship between τ_ϕ and the bulk phase. Mirzadeh et al.²³ derived a new and effective TL model that incorporates surface conduction and connectivity to quantitatively capture the results of the PNP equations. Bazant et al.^{25,26} proposed a porous electrode model that can describe both the micropores inside and the macropores outside a particle, and this model has been widely applied to study the charging dynamics in porous electrodes.^{27,28} A stack-electrode (SE) model^{5,29,30} was recently proposed to successfully bridge the gap between theoretically predicted and experimentally measured τ_ϕ and τ_c . Based on the charging dynamics in individual pores determined using MD simulations,^{11,31–33} effective medium approximation (EMA) can be used to reveal the influences of the pore size distribution and pore connectivity on the charging process of porous electrodes.^{34,35} For example, Henrique et al.³⁶ derived a phenomenological expression for average τ_ϕ as a function of the pore size distribution.

Although the τ_ϕ and τ_c in porous carbon-based electrodes can be easily obtained using the above models with different accuracy levels and calculation costs, these models cannot solve the following two issues simultaneously. First, the real disordered porous structure cannot be intuitively and accurately described using a model. Second, how to quickly calculate τ_ϕ and τ_c using a model and achieve the rapid screening and optimization of porous electrodes is yet unknown. Therefore, a new model based on the above-constructed models is urgently required to more accurately describe and comprehensively optimize the charging dynamics in porous carbon-based electrodes.

In this study, a pore network model (PNM) is introduced to address the above two issues simultaneously, and a self-driven optimization framework is proposed to accelerate the charging dynamics in porous carbon-based electrodes, as shown in Figure 1. The PNM has been applied to the exact modeling of electrochemical devices such as shock electrodialysis,³⁷ Li-ion batteries,³⁸ flow batteries,³⁹ and supercapacitors.⁴⁰ We first proved that the PNM can be easily transformed into the TL and SE models by simplifying its topological structures and geometries. Then, the τ_ϕ and τ_c in the PNM were numerically calculated using the simplified PNP equations and analytically assessed using an equivalent circuit model (ECM). Subsequently, a PNM extracted from a scanning electron microscopic (SEM) image was constructed to verify the analytical solution of τ_ϕ using experimental data. Finally, the optimal pore size distribution of the PNM was revealed using our proposed self-driven optimization framework to accelerate the charging dynamics in porous carbon-based electrodes and guide the design of electrode structures.

2 | RESULTS

2.1 | Relation between the PNM and traditional models

The PNM treats a porous electrode as an ordered or disordered pore network consisting of many different spherical pores and cylindrical throats,⁴¹ as shown in Figure S1a. The geometries and topological structures of the PNM can be directly extracted from a real porous electrode or easily constructed by setting the appropriate structural parameters (Section 4.1.1). Notably, unlike that in the TL and SE models, the bulk phase in the PNM is divided into many cubes to reflect the complex connections between the bulk phase and electrode pores. However, owing to these complex structures, the partial differential equations in the PNM are difficult to solve rapidly using numerical methods. Therefore, we constructed an ECM of the PNM to calculate τ_ϕ and τ_c , as shown in Figure S1b. In the ECM, the nodes represent the bulk phase and pores of porous electrodes, and the lines denote the connections between nodes. The charging relaxation response of a supercapacitor can be modeled using different combinations of capacitors and resistors. The capacitance represents the energy storage capacity of a pore, and the resistance represents the difficulty of ion transport in the pores and bulk phase.

Two generic expressions for τ_ϕ and τ_c are analytically derived based on the ECM (Section 4.1.4). Unlike τ_ϕ , τ_c cannot be derived using the traditional ECM. In this study, we obtained an expression of τ_c by extending the physical meanings of capacitors and resistors in the ECM. The derived expressions demonstrate that τ_ϕ and τ_c are the second-smallest eigenvalues $\lambda_{\min 2}$ of matrices $\mathbf{M}_{(n \times n)}$ and $\mathbf{N}_{(n \times n)}$, respectively:

$$\tau_{\phi, \text{ECM}} = \frac{1}{\min_2(\text{eig}(\mathbf{M}_{(n \times n)}))} = \frac{1}{\min_2\left(\text{eig}\left(\mathbf{C}_{(n \times n)}^{-1} \mathbf{L}_{(n \times n)}^{(G^\Omega)}\right)\right)}, \quad (1a)$$

$$\tau_{c, \text{ECM}} = \frac{1}{\min_2(\text{eig}(\mathbf{N}_{(n \times n)}))} = \frac{1}{\min_2\left(\text{eig}\left(\mathbf{V}_{(n \times n)}^{-1} \mathbf{L}_{(n \times n)}^{(G^d)}\right)\right)}, \quad (1b)$$

where $\min_2(\cdot)$ is the function of the second-smallest value, $\text{eig}(\cdot)$ is the function of the eigenvalues of the matrix, and $^{-1}$ is the operator that inverts the matrix. $\mathbf{C}_{(n \times n)}$ and $\mathbf{V}_{(n \times n)}$ are diagonal matrices with the weights of each pore's capacitance C and volume V , respectively. $\mathbf{L}_{(n \times n)}^{G^\Omega}$ and $\mathbf{L}_{(n \times n)}^{G^d}$ are Laplacian matrices with the weights of each throat's ionic conductance G^Ω and diffusive conductance G^d , respectively. $\mathbf{M}_{(n \times n)}$ and $\mathbf{N}_{(n \times n)}$ contain all the heterogeneous structural parameters of the pore network, including the position, connectivity, and geometric parameters of individual pores and throats as well as some properties of the electrolyte, including the initial concentration and diffusion coefficient of ions. The expressions of C , G^Ω , and G^d are detailed in Equation (3). Interestingly, Equation (1) indicates that τ_ϕ and τ_c have similar forms, which inspires us to believe that the relaxation time of temperature τ_T can be obtained in the same manner.³⁰

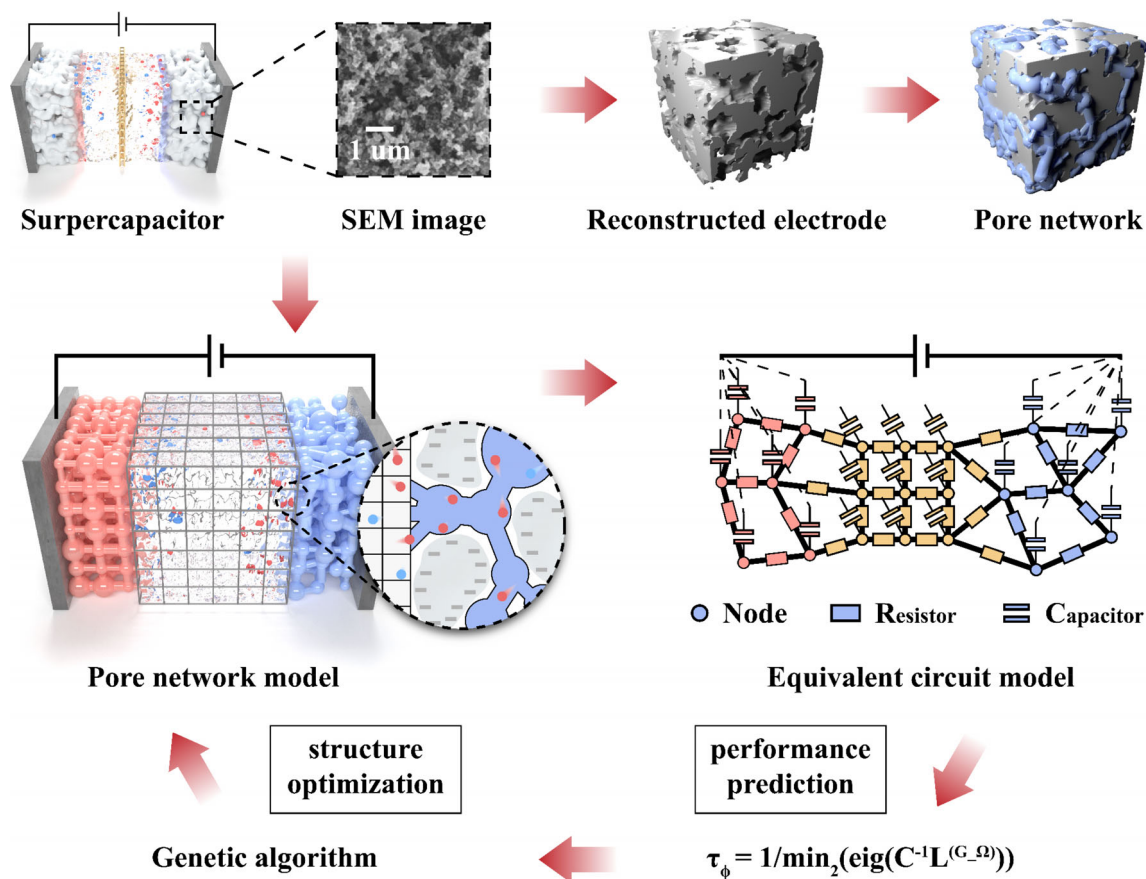


FIGURE 1 Self-driven optimization framework for investigating the charging dynamics in porous electrodes. The simulated annealing algorithm is first used to reconstruct the three-dimensional structure of a porous carbon-based electrode from a two-dimensional scanning electron microscopic (SEM) image of a supercapacitor. The pore network of the pore phase is then extracted from the reconstructed electrode using the maximal ball algorithm. Subsequently, the pore network model of the supercapacitor, which contains two porous carbon-based electrodes and a bulk phase, is constructed based on the extracted pore network. The relaxation time τ expressions are derived using an equivalent circuit model of the pore network model (PNM) to accurately and rapidly characterize the time scale at which the charge, potential, or concentration reaches equilibrium. Finally, the genetic algorithm and derived expression are combined to automatically search the minimum τ by optimizing the geometries and topological structure of the PNM to accelerate the charging dynamics in porous electrodes.

The PNM can be downward-transformed into the TL and SE models by simplifying the topological structure and geometry, as shown in Figure S1c,d. Therefore, τ_ϕ and τ_c in the TL and SE models can be calculated using Equation (1) by taking the corresponding C , G^Ω , and G^d , as listed in Table S1. For example, based on the TL model, Mirzadeh et al.²³ simplified a disordered porous structure into a cylindrical pore with a sectional area A , sectional perimeter P , and length L by considering that ions are transported along the axial direction of the cylindrical pore and adsorbed on the pore wall to form an EDL. The expression of τ_ϕ derived from the TL model is $\tau_{\phi,TL} = \frac{PL}{A} \tau_{RC}$, where τ_{RC} is the charging τ of the plate electrode. In the SE model, the porous electrode is simplified into n infinitely large plate electrodes stacked in parallel,⁵ and the gap between plates is considered the average pore size h . The thickness of the porous electrode is $H = (n-1)h$ and the length of the bulk phase is $2L$. Ions can be transported through the plate or adsorbed on either side of it. The expression of $\tau_{\phi,SE}$ derived from the SE model is $\tau_{\phi,SE} = [(2 + 0.75 \frac{H}{h})n - 1 - 0.91 \frac{H}{h}] \tau_{RC}$. However, the TL and SE models ignore the microscopic disordered details of the

topological structure and geometries of disordered carbon-based electrodes. For the EMA, the topological structure is approximately replaced by a mathematical expression of a single pore to represent the disordered porous structure on a statistical level, considering only the influence of connectivity and pore size distribution, as shown in Figure S1e. The PNM can be simplified into an EMA when the bulk phase and heterogeneous details of the electrodes are ignored.

2.2 | Relaxation times from the PNM

The simplified PNP equations are used to numerically solve the distributions of potential ϕ and ionic concentration c in the PNM during the charging process (Section 4.1.2) and calculate τ_ϕ and τ_c from the numerical results (Section 4.1.3). To visualize the numerical results, we selected four snapshots of the potential distribution at $\{0, 0.1, 1, 10\} \tau_\phi$ and concentration distribution at $\{0, 0.1, 1, 10\} \tau_c$, as shown in Figure 2A,B. At time $t = 0$ s, a potential difference 2ψ is applied to the

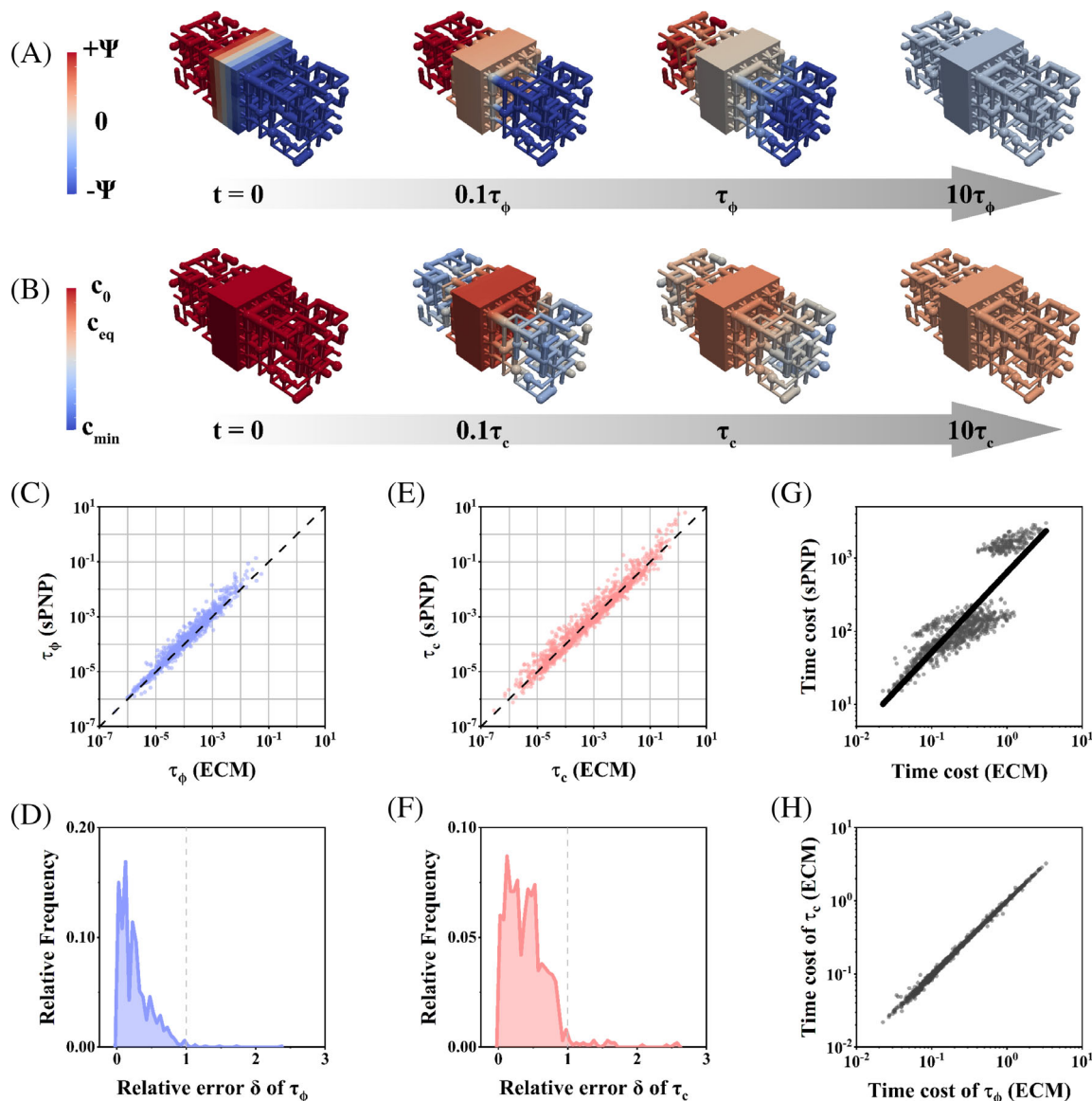


FIGURE 2 Relaxation process and relaxation times τ . (A, B) Snapshots of the potential distribution at $\{0, 0.1, 1, 10\}\tau_\phi$ and concentration distribution at $\{0, 0.1, 1, 10\}\tau_c$, where τ_ϕ and τ_c are the τ of the potential and concentration, respectively. (C, E) Comparison between the analytical solutions τ_{ECM} obtained from the pore network model (PNM)-derived equivalent circuit model (ECM) and numerical solutions τ_{sPNP} calculated using the simplified Poisson–Nernst–Planck (PNP) equations. (D, F) Distributions of the absolute values of the relative errors of ECM $\delta = |(\tau_{\text{ECM}} - \tau_{\text{sPNP}})/\tau_{\text{sPNP}}|$. (G, H) Comparison between the time costs of the PNM-derived ECM and the simplified PNP equations.

cathode and anode of the supercapacitor with a homogeneous ionic concentration c_0 . Over time, the counterions are adsorbed onto the electrode surface whereas the co-ions are repulsed such that EDLs gradually form. These EDLs screen the surface potentials, leading to electroneutrality. Meanwhile, ions from the bulk electrolyte enter the porous electrode to gradually replenish the ions adsorbed by the surface. The potential at $0.1\tau_\phi$ and concentration at $0.1\tau_c$ are far from equilibrium, whereas the potential at $10\tau_\phi$ and concentration at $10\tau_c$ are in equilibrium. Therefore, τ_ϕ and τ_c can represent the time scales at which the potential and concentration reach equilibrium. Figure S2a,b illustrate that the variations in ϕ and c obtained by the PNM show complex behaviors rather than an exponential relation, as commonly reported.⁵ This anomalous phenomenon is ascribed to the

disordered structure of the carbon-based porous electrodes and mass transport between pores.

Supporting Information Material Section S2 discusses the effects of the parameters of disordered porous structures on τ_ϕ and τ_c , which are ignored in the TL model, SE model and EMA. We adopted the numerical solutions to ensure higher accuracy for τ_ϕ and τ_c . The studied structural parameters include the standard deviation of the pore size σ (i.e., the disorder of the pore size), the average connectivity of the electrode Z , and the pore arrangement controlled by random seed ω (i.e., the microscopic surface topography). When $\sigma = 0$, $Z_{\text{cathode}} = Z_{\text{anode}} = 2$, and the pore arrangement is ignored, the results of the PNM can be regarded as those of the TL model, SE model, and EMA. These results show that σ has great positive influences

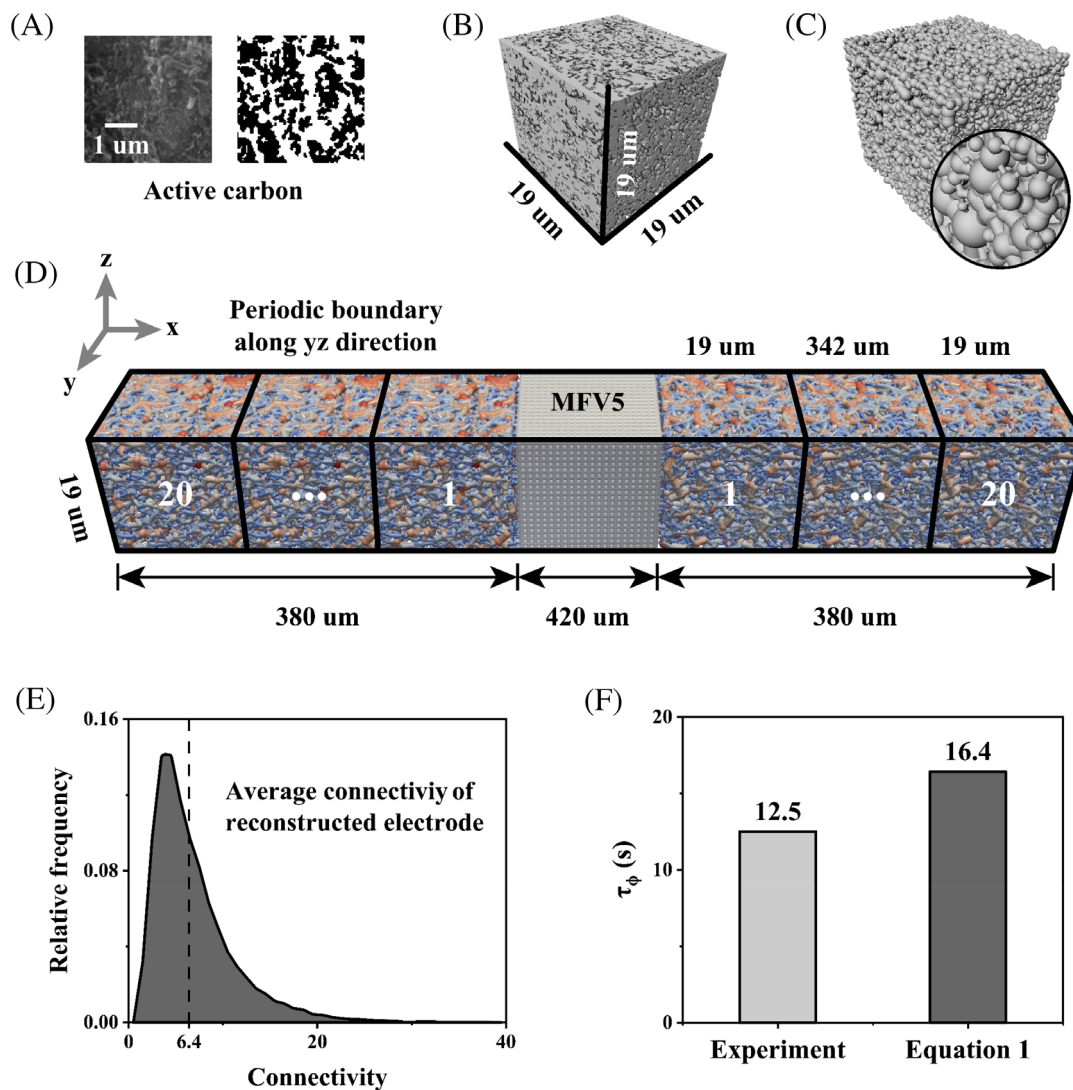


FIGURE 3 Relaxation time in a real porous electrode. (A) Scanning electron microscopic image of active carbon obtained from a previous experiment and the corresponding binary segmentation results. The white region refers to the pore phase, and the black region refers to the solid phase. (B) Reconstructed electrode obtained using the simulated annealing algorithm. (C) Pore network of the pore phase extracted from (B). (D) pore network model (PNM) of a supercapacitor composed of an active carbon electrode and glass microfiber (MFV5) separator. (E) Distribution of the connectivity of (C). (F) Comparison between the experimental and analytical τ_ϕ .

on τ_ϕ and τ_c , indicating that a disordered pore size distribution results in slow charging dynamics. Moreover, as both Z_{cathode} and Z_{anode} increase, τ_ϕ and τ_c first decrease sharply until $Z_{\text{cathode}} = Z_{\text{anode}}$, after which their rate of descent slows. More interestingly, even when σ and Z are held constant, the pore arrangement exerts significant influences on τ_ϕ and τ_c . Specifically, the distribution of 500 types of pore arrangements in electrodes of the same size indicates that the maximum τ_ϕ and τ_c are over two times greater than the minimum values.

In Figure 2C–H, we compare the analytical solutions τ_{ECM} (i.e., Equation 1) derived by the ECM and the numerical solutions τ_{SPNP} (i.e., Equation 5) calculated using the simplified PNP equations in terms of accuracy and time cost. Figure 2C,E shows the distribution of points; here, the abscissa is τ_{ECM} and the ordinate is τ_{SPNP} . The points are evenly distributed on both sides of $y = x$. Specifically,

most of the absolute values of the relative error δ of the ECM are less than 1 for both τ_ϕ and τ_c , where $\delta = |(\tau_{\text{ECM}} - \tau_{\text{SPNP}}) / \tau_{\text{SPNP}}|$, as shown in Figure 2D,F. Therefore, τ_ϕ and τ_c could be calculated by Equation (1) with high accuracy. More importantly, the time cost of the ECM is approximately 1000 times lower than that of the PNM, as shown in Figure 2G. Besides, Figure 2H indicates the ECM has the same efficiency for solving τ_ϕ and τ_c . To find the key parameters for δ , we studied the influences of various parameters of the PNM on δ . In Figure S9, we found that $\delta(\tau_\phi) \sim Z_{\text{sq}}^{-3.6}$ and $\delta(\tau_c) \sim Z_{\text{sq}}^{-0.2}$ and that other parameters have a weak influence on both $\delta(\tau_\phi)$ and $\delta(\tau_c)$, where $Z_{\text{sq}} = \sqrt{Z_{\text{cathode}} Z_{\text{anode}}}$. Thus, we can conclude that increases in Z_{sq} improve the accuracy of the analytical solution. Because a higher Z_{sq} allows for the easier transport of ions through each pore, resulting in a more uniform concentration distribution, the assumptions used to derive τ_ϕ and τ_c (i.e., C and R are constant) are reasonable.

2.3 | Validation of the PNM results using experimental evaluation

To further validate the accuracy of Equation (1), we compared the analytical solution of τ_ϕ with its experimental solution. Because the topological structure of practical carbon-based electrodes is disordered and the average properties (such as the pore size distribution) cannot elucidate the significance of heterogeneous structural parameters, setting the geometric parameters either randomly or according to a normal distribution is not reasonable. Therefore, we constructed a disordered pore network from a real carbon-based electrode, as shown in Figure 3, to bridge the PNM with the real structure.

At present, the structure of porous media can be obtained nondestructively using computed tomography (CT)⁴² and SEM.⁴³ However, CT cannot easily resolve structures less than half a micron in size, and SEM has the disadvantage of providing only two-dimensional (2D) information. An effective method for obtaining the 3D structure of porous electrodes based on SEM images is random reconstruction, such as the simulated annealing (SA) algorithm⁴⁴ or machine learning.⁴⁵ The SA algorithm can reconstruct a porous electrode from the SEM image segmentation results (Section 4.2). Figure 3A,B show SEM images of active carbon obtained from an experiment⁴⁶ and the reconstructed active carbon electrode, respectively. The reconstructed electrode preserves the details of the active carbon to the greatest extent possible. The maximal ball algorithm (Section 4.3) was then adopted to convert the reconstructed electrode into a disordered pore network, as shown in Figure 3C. The PNM of the supercapacitor⁴⁶ was constructed based on the extracted pore network, as shown in Figure 3D. The thicknesses of the electrode and separator are 0.38 and 0.42 mm, respectively. The cathode and anode comprise 20 extracted pore networks, thereby satisfying the actual thickness of the electrodes. In addition, periodic boundary conditions were imposed along the yz direction to reflect actual conditions. Detailed parameters are listed in Table S5.

Figure 3E shows that the Z of the reconstructed electrode is 6.4; thus, Equation (1a) is sufficiently accurate to calculate τ_ϕ because $\delta(\tau_\phi) \sim Z_{sq}^{-3.6}$. Using Equation (1a), we found that $\tau_\phi = 16.4$ s, which is roughly within one order of magnitude relative to the relaxation time (12.5 s) observed in the experimental data,⁴⁶ as shown in Figure 3F. Given the simplicity of the governing equations, the remaining discrepancies are not surprising. Therefore, the influence of the pore structure of porous carbon-based electrodes on the charging dynamics can be well described by the PNM.

2.4 | Accelerating charging dynamics using the self-driven optimization framework

The structure of porous electrodes determines the charging time scale of supercapacitors, as shown in Figures S7 and S8. However, the empirical design of electrodes is expensive, time- and labor-intensive, and limited to a narrow design space determined by the existing manufacturing routes. To guide the experimental design of electrodes and accelerate material discovery, we used the self-driven optimization

framework to explore the optimal structure of the PNM. Compared with the traditional gradient descent method, the genetic algorithm (Section 4.4) does not need to consider whether the objective function is differentiable and can be directly computed iteratively.⁴⁷

Figure 4 exhibits a simple example of our proposed framework, which aims to accelerate the charging dynamics (i.e., minimize τ_ϕ) by optimizing the pore size distribution of the electrodes in Figure 3C. The initial and optimized structures are shown in Figure 4A,B, respectively. Notably, the porosity of the electrode did not change after optimization. The pore size distribution is controlled by changing the size of each pore in the electrodes rather than the form of the distribution function. Figure 4C presents the optimization procedure of τ_ϕ . As the number of iterations increases, τ_ϕ decreases from an initial value of 5.37×10^{-2} s to the optimal value of 5.04×10^{-2} s. Therefore, when the pore size distribution of the electrodes is optimized, τ_ϕ drops to 94% of its initial value. Finally, we compared the pore size distributions before and after optimization, as shown in Figure 4D. The results show that an appropriate reduction in pore size can accelerate the charging dynamics of the electrode. In addition, adjusting the form of the pore size distribution is an effective means to decrease τ_ϕ , as shown in Figure S11. The results indicate that the pore size distribution evolves from an initial normal distribution to a bimodal one and that τ_ϕ drops to 41% of its initial value. Numerous experiments have demonstrated that porous electrodes with bimodal distributions can accelerate the charging dynamics of supercapacitors.^{48–50} However, determining the optimal form of a bimodal distribution using only a few sets of experiments is difficult. Fortunately, the optimization framework proposed in this work can quickly determine optimal structural parameters, such as the pore size distribution, connectivity distribution, and porosity, as well as electrolyte properties.

3 | DISCUSSION

In this work, we introduced a PNM to study and accelerate the charging dynamics in porous carbon-based electrodes via self-driven optimization. An ECM of the PNM was constructed to quantitatively describe the influence of the disordered structure of the PNM on the charging process, which was then compared with the results of numerical calculations using simplified PNP equations. Using the ECM, we proposed a simple mathematical expression that considers the effects of electrolyte properties and disordered electrode structures to quantify τ_ϕ and τ_c . We found that this expression can be simplified into expressions derived from other widely used models, such as the TL and SE models. This expression was verified using numerical solutions and experimental data, with relative errors of less than 100% and 30%, respectively. According to the numerical solutions, increasing σ results in slow charging dynamics owing to the disordered pore size distribution. In addition, increasing Z_{cathode} and Z_{anode} can reduce τ_ϕ and τ_c to accelerate the charging dynamics. More interestingly, even when σ and Z are kept constant, the pore arrangement (i.e., microscopic surface topography) exerts significant influences on the ranges of τ_ϕ and τ_c ; these influences cannot easily be described using traditional models. Finally, we proposed a self-driven optimization framework by coupling our

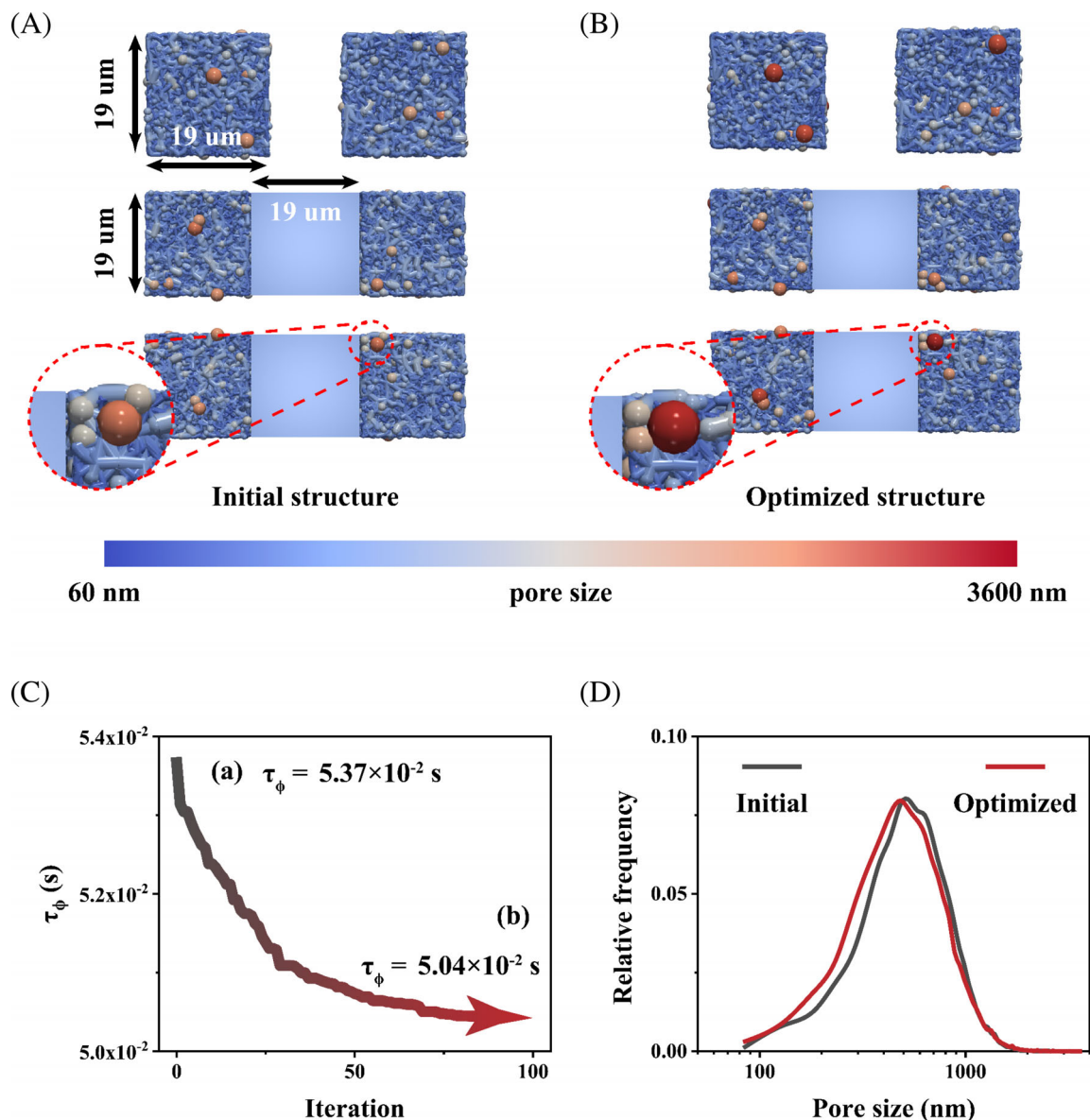


FIGURE 4 Optimization of the pore network model structure using the self-driven optimization framework to minimize τ_ϕ . (A) Initial structure. (B) Optimized structure with the same porosity as in (A). (C) Minimum τ_ϕ for each iteration. (D) Pore size distributions before and after optimization.

derived expression with a genetic algorithm to accelerate the charging dynamics in porous carbon-based electrodes by optimizing their structural parameters. For example, τ_ϕ can decrease to 96% of its initial value by searching for the optimal pore size distribution. Moreover, to decrease τ_ϕ and τ_c , we could (1) increase Z and the A of electrode by calendaring the electrode, (2) reduce σ by changing the synthesis process, or (3) change the microscopic surface topography. Therefore, our study provides a general platform for understanding and optimizing the charging dynamics of porous carbon-based electrodes.

In the future, more accurate governing equations, such as the modified PNP equations that consider the size of ions, could be used in the PNM to achieve more realistic simulations in systems with smaller pore sizes.^{51,52} Furthermore the process of electrode fabrication and process simulation methods, such as the discrete element

method,⁵³ could be incorporated into the existing framework to achieve optimized porous structures.

4 | METHODS

4.1 | Pore network model

4.1.1 | Pore networks of the electrode and bulk phase

The fundamental tenet of PNM is that the pore phase of the porous electrode and the bulk phase are regarded as a pore network consisting of many pores and throats.⁴¹ The PNM can be transformed into

the random resistor networks⁵⁴ and percolation models⁵⁵ by removing the pores. The total volume of all pores in the pore phase determines the porosity of porous electrodes. Throats are both relatively long, narrow channels connecting pores in the electrode and concise channels in the bulk phase, which can be regarded as capillary tubes for ion transport. Connectivity is defined as the number of throats connected to the pores. In this work, ball-and-stick and cube-and-cuboid models were used to characterize the pore networks of the porous electrodes and bulk phase, respectively, as shown in Figure S1a.

The default structural parameters of the pore networks are set as follows. The topological structure is a cubic isometric network, as shown in the red portion of the PNM in Figure 1. The spaces between the nodes in the electrode and bulk phases are 100 and 50 nm, respectively. The dimensions of both the cathode and anode are $5 \times 5 \times 5$. The size of the bulk phase is $10 \times 10 \times 10$. The pore sizes satisfy a normal distribution (the average pore size is 50 nm, and σ is 10 nm). Z_{cathode} and Z_{anode} are both 2.5. ω Controls the pore arrangement, and the default value is zero. All PNMs were generated using the Python package *OpenPNM*.

4.1.2 | Governing equations and initial conditions

The local electrostatic potential $\phi(x,t)$ and local ionic concentration $c(x,t)$ are modeled using the simplified PNP equations,⁴⁰ which are appropriate for obtaining the linear response of supercapacitors with small salt concentration gradients. The simplified equations assume electroneutrality in the pores, a monovalent salt solution, and identical diffusion coefficients for both anions and cations. The corresponding electrostatic potential $\phi_i(t)$ and ionic concentration $c_i(t)$ in pore i are described by the PNM as follows:

Porous electrode

$$C_i \frac{\partial \phi_i}{\partial t} = - \sum_{j=1}^{Z_i} G_{ij}^{\Omega} (\phi_i - \phi_j), \quad (2a)$$

$$V_i \frac{\partial c_i}{\partial t} = - \sum_{j=1}^{Z_i} G_{ij}^d (c_i - c_j) - \frac{C_i}{2z^{\text{count}}F} \frac{\partial \phi_i}{\partial t}. \quad (2b)$$

Bulk phase

$$0 = - \sum_{j=1}^{Z_i} G_{ij}^{\Omega} (\phi_i - \phi_j), \quad (2c)$$

$$V_i \frac{\partial c_i}{\partial t} = - \sum_{j=1}^{Z_i} G_{ij}^d (c_i - c_j), \quad (2d)$$

where C_i is the capacitance of pore i , V_i is the volume of pore i , Z_i is the connectivity of pore i , z^{count} is the counterion valence, F is the Faraday constant, G_{ij}^d is the diffusive conductance between pores i and j , and G_{ij}^{Ω} is the ionic conductance between pores i and j ,

respectively. Notably, z^{count} is +1 in the cathode and -1 in the anode for a monovalent salt solution. C_i and G_{ij}^{tr} (where tr is d or Ω) are defined as:

$$C_i = S_i \epsilon_0 \epsilon_r \lambda_{D,i}^{-1}, \quad (3a)$$

$$G_{ij}^{\text{tr}} = \left(\frac{1}{g_i^{\text{tr}}} + \frac{1}{g_j^{\text{tr}}} + \frac{1}{g_{ij}^{\text{tr}}} \right)^{-1}, \quad (3b)$$

$$g_i^d = \frac{DA_i}{l_i}, \quad (3c)$$

$$g_i^{\Omega} = \frac{2F^2 c_i}{RT} g_i^d = \frac{2F^2 DA_i c_i}{RT l_i}, \quad (3d)$$

where S_i is the surface area of pore i minus the cross-sectional area of throat ij , ϵ_0 is the permittivity of a vacuum, ϵ_r is the relative permittivity of the solution, $\lambda_{D,i} = \sqrt{(\epsilon_0 \epsilon_r RT) / (2F^2 c_i)}$ is the Debye length of pore i , D is the diffusion coefficient of the ions, A_i is the cross-sectional area of pore i or throat ij , l_i is the length of pore i or throat ij , R is the ideal gas constant, and T is the temperature. Equation (3b) shows that the conductance of each pore–throat–pore conduit consists of three parts. The structural parameters of each part of the conduit, such as A_i and l_i , are explained in detail in Figure S3.

Initially, the ionic concentration is homogeneous, and the electric potentials $+\Psi$ and $-\Psi$ are applied to the cathode and anode, respectively:

I.C.

$$c_i(t=0) = c_0, \quad (4a)$$

$$\phi_{\text{cathode}}(t=0) = +\Psi = vV_m, \quad (4b)$$

$$\phi_{\text{anode}}(t=0) = -\Psi = -vV_m, \quad (4c)$$

where c_0 is the initial ionic concentration, v is the scale factor of the thermal voltage, $V_m = (k_B T) / e$ is the thermal voltage, k_B is the Boltzmann constant, and e is the elementary charge.

We use the following default parameter set: $z_+ = -z_- = 1$, $T = 298.15$ K, $D = 2 \times 10^{-9}$ m²/s, $\epsilon_r = 71$, and $c_0 = 100$ mol/m³. Therefore, the initial λ_D and V_m are equal to 9.15×10^{-10} m and 0.02526 V, respectively. The above governing equations were solved for specific initial conditions over $10^{-5} \tau_\phi - 10^2 \tau_c$ using the COMSOL *Multiphysics* finite element-based solver.

4.1.3 | Numerical calculation for the relaxation time scales in the PNM

To characterize the different time responses observed during the potential–concentration coupled charging dynamics, we adopt τ to describe the point at which the potential and concentration reach

equilibrium. According to a purely exponential charge buildup,^{5,30} the time-dependent functions $\tau_{\phi,i}(t)$ and $\tau_{c,i}(t)$ in pore i are defined as:

$$\tau_{\phi,i}(t) = - \left\{ \frac{d \ln [1 - (\phi - \phi_{\text{eq}}) / (\phi_0 - \phi_{\text{eq}})]}{dt} \right\}^{-1}, \quad (5a)$$

$$\tau_{c,i}(t) = - \left\{ \frac{d \ln [1 - (c - c_{\text{eq}}) / (c_0 - c_{\text{eq}})]}{dt} \right\}^{-1}, \quad (5b)$$

$$\tau_{\phi,\text{sPNP}} = \max(\tau_{\phi,i} | \tau_{\phi,i}(t) = t), \quad (5c)$$

$$\tau_{c,\text{sPNP}} = \max(\tau_{c,i} | \tau_{c,i}(t) = t), \quad (5d)$$

where subscripts eq and 0 represent the equilibrium and initial states, respectively.³⁰ Figure S2c,d shows the $\tau_{\phi,i}(t)$ and $\tau_{c,i}(t)$ in the porous electrode and bulk phase, respectively. τ_i is equal to the values corresponding to the intersection of $\tau_i(t)$ and $y=x$. The relaxation times of the system (i.e., τ_{ϕ} and τ_c) are defined as the maximum $\tau_{\phi,i}$ and $\tau_{c,i}$ in all pores.

4.1.4 | Analytical solution of the ECM of the PNM

To provide an accurate description of the influence of the PNM parameters, especially τ , on the charging dynamics, we introduce an ECM of the PNM, as shown in Figures S1b and S4. Notably, in this study, the capacitance of the bulk phase is zero because the bulk phase cannot absorb ions. In addition, C and G are hypothetically independent of time. However, only τ_{ϕ} can be obtained by classical ECM,^{5,24} as shown in Figure S4a. To calculate τ_c , we extend the ECM by changing the physical meaning of capacitors and resistors. Specifically, in the case of concentration, the capacitance is equal to the pore volume and the resistance is the reciprocal of the diffusive conductance of the conduit, as shown in Figure S4b. Section S1 details the derivation of Equation (1), which mainly focuses on the potential, and the concentration is obtained simply by substituting the corresponding place. Currently, the algebraic form of Equation (1) cannot be obtained. Therefore, the second-smallest eigenvalue of the matrix was solved using the Python package *SciPy*.

4.2 | SA algorithm: Reconstruction of real porous electrodes

A nested multiresolution hierarchical SA algorithm⁴⁴ was used to reconstruct the porous electrode from SEM images. This algorithm can capture the features of the long-range connectivity of samples with a low computational burden. The reconstruction process is as follows: (1) scan the porous electrode using SEM to obtain the reference image; (2) identify the solid and pore phases of the reference image using image segmentation; (3) generate a random initial 3D voxel point cloud with the same porosity as the reference image; (4) use the SA algorithm to reconstruct the point cloud randomly by changing the phase of a voxel (solid or pore) so that its features gradually resemble the reference image; and (5) transform the voxel point cloud

into volumetric data from the pore and solid phases. The parameter setup of the algorithm is presented in Table S3. The code for the algorithm is obtained from the literature.⁴⁴

4.3 | Maximal ball algorithm: Extraction of pore networks from real porous electrodes

The maximal ball algorithm is a morphological analysis method used to extract a network of pores and throats from volumetric data.⁵⁶ The extraction process is as follows: (1) extract the representative elementary volume (REV) of the pore phase; (2) select any voxel point in the REV and search for the adjacent voxel points in specific directions around it; (3) use the shrinkage algorithm to find the maximum ball as well as the upper and lower limits of its radius according to the formation range of the voxels to determine the size and position of the maximum ball; (4) continue to find the next maximum ball according to the above method; and (5) classify all maximum balls into pores or throats. The parameter setup of the algorithm, which was implemented using the software Avizo, is shown in Table S4.

4.4 | Genetic algorithm: Optimization of the PNM structure

The self-driven optimization framework coupling Equation (1) and the genetic algorithm are shown in Figure S10. The concept of a genetic algorithm is based on the evolution of a population of candidate solutions to a given design case using operators based on natural diversity and selection.⁴⁷ The process of optimization is as follows: (1) initialize individuals (i.e., a certain type of pore arrangement) and populations (i.e., many types of pore arrangements) and encode them; (2) before the termination conditions satisfied, calculate the fitness of the decoded individual, parent selection, crossover, and mutation; and (3) after termination, select the individual with the best fitness (i.e., the optimal pores arrangements) as the optimal solution. The parameter setup for the algorithm is listed in Table S6. The genetic algorithm was implemented using the Python package *Geatpy*.

AUTHOR CONTRIBUTIONS

Pan Huang: Conceptualization (equal); data curation (lead); formal analysis (lead); investigation (lead); methodology (lead); software (lead); validation (lead); visualization (lead); writing – original draft (lead); writing – review and editing (lead). **Haolan Tao:** Supervision (supporting); writing – original draft (equal); writing – review and editing (equal). **HongLai Liu:** Funding acquisition (equal); project administration (equal); resources (equal); supervision (equal). **Cheng Lian:** Conceptualization (lead); project administration (equal); resources (equal); supervision (equal); writing – original draft (equal); writing – review and editing (equal).

ACKNOWLEDGMENTS

This work was supported by the National Key R&D Program of China (No. 2022YFA1503501), the National Natural Science Foundation of

China (No. 22278127 and 22078088), the Fundamental Research Funds for the Central Universities (No. 2022ZFJH004), the Shanghai Rising-Star Program (No. 21QA1401900), and Jiangsu Engineering Laboratory of New Materials for Sewage Treatment and Recycling. We kindly thank Jie Yang and Yiting Lin for their helpful discussions.

CONFLICT OF INTEREST STATEMENT

The authors declare no conflict of interest.

DATA AVAILABILITY STATEMENT

The simulated data presented in this work are available from the corresponding authors upon reasonable request.

ORCID

Haolan Tao  <https://orcid.org/0000-0003-4436-9144>

Cheng Lian  <https://orcid.org/0000-0002-9016-832X>

REFERENCES

- Forse AC, Griffin JM, Merlet C, et al. Direct observation of ion dynamics in supercapacitor electrodes using in situ diffusion NMR spectroscopy. *Nat Energy*. 2017;2(3):16216.
- Wang Q, Yan J, Fan Z. Carbon materials for high volumetric performance supercapacitors: design, progress, challenges and opportunities. *Energy Environ Sci*. 2016;9(3):729-762.
- Yang Z, Zhang J, Kintner-Meyer MCW, et al. Electrochemical energy storage for green grid. *Chem Rev*. 2011;111(5):3577-3613.
- Zhu C, Du D, Eychmüller A, Lin Y. Engineering ordered and nonordered porous noble metal nanostructures: synthesis, assembly, and their applications in electrochemistry. *Chem Rev*. 2015;115(16):8896-8943.
- Lian C, Janssen M, Liu H, van Roij R. Blessing and curse: how a supercapacitor's large capacitance causes its slow charging. *Phys Rev Lett*. 2020;124(7):076001.
- Xia H, Zhang W, Cao S, Chen X. A figure of merit for fast-charging Li-ion battery materials. *ACS Nano*. 2022;16(6):8525-8530.
- Fuller TF, Doyle M, Newman J. Relaxation phenomena in lithium-ion-insertion cells. *J Electrochem Soc*. 1994;141(4):982-990.
- Koresh J, Soffer A. Double layer capacitance and charging rate of ultramicroporous carbon electrodes. *J Electrochem Soc*. 1977;124(9):1379-1385.
- Gargh P, Sarkar A, Lui YH, et al. Correlating capacity fade with film resistance loss in fast charging of lithium-ion battery. *J Power Sources*. 2021;485:229360.
- Yang J, Janssen M, Lian C, van Roij R. Simulating the charging of cylindrical electrolyte-filled pores with the modified Poisson-Nernst-Planck equations. *J Chem Phys*. 2022;156(21):214105.
- Kondrat S, Wu P, Qiao R, Kornyshev AA. Accelerating charging dynamics in subnanometre pores. *Nat Mater*. 2014;13(4):387-393.
- Bazant MZ, Thornton K, Ajdari A. Diffuse-charge dynamics in electrochemical systems. *Phys Rev E Stat Nonlin Soft Matter Phys*. 2004;70(2):021506.
- Tivony R, Safran S, Pincus P, Silbert G, Klein J. Charging dynamics of an individual nanopore. *Nat Commun*. 2018;9(1):4203.
- Rubin S, Suss ME, Biesheuvel PM, Bercovici M. Induced charge capacitive deionization: the electrokinetic response of a porous particle to an external electric field. *Phys Rev Lett*. 2016;117(23):234502.
- Bi S, Banda H, Chen M, et al. Molecular understanding of charge storage and charging dynamics in supercapacitors with MOF electrodes and ionic liquid electrolytes. *Nat Mater*. 2020;19:552-558.
- Feng G, Chen M, Bi S, et al. Free and bound states of ions in ionic liquids, conductivity, and underscreening paradox. *Phys Rev X*. 2019;9(2):021024.
- Mai W, Yang M, Soghrati S. A particle-resolved 3D finite element model to study the effect of cathode microstructure on the behavior of lithium ion batteries. *Electrochim Acta*. 2019;294:192-209.
- Tao H, Lian C, Liu H. Multiscale modeling of electrolytes in porous electrode: from equilibrium structure to non-equilibrium transport. *Green Energy Environ*. 2020;5(3):303-321.
- Song J, Bazant MZ. Electrochemical impedance imaging via the distribution of diffusion times. *Phys Rev Lett*. 2018;120(11):116001.
- de Levie R. On porous electrodes in electrolyte solutions. *Electrochim Acta*. 1963;8(10):751-780.
- Peon C, Rotenberg B, Simon P, Salanne M. Multi-scale modelling of supercapacitors: from molecular simulations to a transmission line model. *J Power Sources*. 2016;326:680-685.
- Gupta A, Zuk PJ, Stone HA. Charging dynamics of overlapping double layers in a cylindrical nanopore. *Phys Rev Lett*. 2020;125(7):076001.
- Mirzadeh M, Gibou F, Squires TM. Enhanced charging kinetics of porous electrodes: surface conduction as a short-circuit mechanism. *Phys Rev Lett*. 2014;113(9):097701.
- Janssen M. Transmission line circuit and equation for an electrolyte-filled pore of finite length. *Phys Rev Lett*. 2021;126(13):136002.
- Biesheuvel PM, Fu Y, Bazant MZ. Diffuse charge and faradaic reactions in porous electrodes. *Phys Rev E Stat Nonlin Soft Matter Phys*. 2011;83(6):061507.
- Biesheuvel PM, Fu Y, Bazant MZ. Electrochemistry and capacitive charging of porous electrodes in asymmetric multicomponent electrolytes. *Russ J Electrochem*. 2012;48(6):580-592.
- He F, Biesheuvel PM, Bazant MZ, Hatton TA. Theory of water treatment by capacitive deionization with redox active porous electrodes. *Water Res*. 2018;132:282-291.
- Singh K, Bouwmeester HJM, de Smet LCPM, Bazant MZ, Biesheuvel PM. Theory of water desalination with intercalation materials. *Phys Rev Appl*. 2018;9(6):064036.
- Lin Y, Lian C, Berrueta MU, Liu H, van Roij R. Microscopic model for cyclic voltammetry of porous electrodes. *Phys Rev Lett*. 2022;128(20):206001.
- Huang P, Tao H, Yang J, Lian C, Liu H. Four stages of thermal effect coupled with ion-charge transports during the charging process of porous electrodes. *AIChE J*. 2022;68:e17790.
- Jeanmairet G, Rotenberg B, Salanne M. Microscopic simulations of electrochemical double-layer capacitors. *Chem Rev*. 2022;122(12):10860-10898.
- Feng G, Li S, Presser V, Cummings PT. Molecular insights into carbon supercapacitors based on room-temperature ionic liquids. *J Phys Chem Lett*. 2013;4(19):3367-3376.
- Scalfi L, Salanne M, Rotenberg B. Molecular simulation of electrode-resolution interfaces. *Annu Rev Phys Chem*. 2021;72(1):189-212.
- Tao H, Chen G, Lian C, Liu H, Coppens MO. Multiscale modeling of ion transport in porous electrodes. *AIChE J*. 2022;68(4):e17571.
- Lian C, Su H, Li C, Liu H, Wu J. Non-negligible roles of pore size distribution on electroosmotic flow in Nanoporous materials. *ACS Nano*. 2019;13(7):8185-8192.
- Henrique F, Zuk PJ, Gupta A. Charging dynamics of electrical double layers inside a cylindrical pore: predicting the effects of arbitrary pore size. *Soft Matter*. 2022;18(1):198-213.
- Alizadeh S, Bazant MZ, Mani A. Impact of network heterogeneity on electrokinetic transport in porous media. *J Colloid Interface Sci*. 2019;553:451-464.
- Khan ZA, Agnaou M, Sadeghi MA, Elkamel A, Gostick JT. Pore network modelling of galvanostatic discharge behaviour of lithium-ion battery cathodes. *J Electrochem Soc*. 2021;168(7):070534.
- Sadeghi MA, Aganou M, Kok M, et al. Exploring the impact of electrode microstructure on redox flow battery performance using a multiphysics pore network model. *J Electrochem Soc*. 2019;166(10):A2121-A2130.

40. McKague M, Fathiannasab H, Agnaou M, Sadeghi MA, Gostick J. Extending pore network models to include electrical double layer effects in micropores for studying capacitive deionization. *Desalination*. 2022;535:115784.
41. Gostick J, Aghighi M, Hinebaugh J, et al. OpenPNM: a pore network modeling package. *Comput Sci Eng*. 2016;18(4):60-74.
42. Gc C, Mw V. Noninvasive three-dimensional computer imaging of matrix-filled fossil skulls by high-resolution computed tomography. *Science*. 1984;226(4673):456-458.
43. Kunanusont N, Shimoyama Y. Porous carbon electrode for Li-air battery fabricated from solvent expansion during supercritical drying. *J Supercrit Fluids*. 2018;133:77-85.
44. Lemmens L, Rogiers B, Jacques D, et al. Nested multiresolution hierarchical simulated annealing algorithm for porous media reconstruction. *Phys Rev E Stat Nonlin Soft Matter Phys*. 2019;100(5):053316.
45. Xu H, Zhu J, Finegan DP, et al. Guiding the design of heterogeneous electrode microstructures for Li-ion batteries: microscopic imaging, predictive modeling, and machine learning. *Adv Energy Mater*. 2021;11(19):2003908.
46. Daraghmeah A, Hussain S, Haq AU, Saadeddin I, Servera L, Ruiz J. Carbon nanocomposite electrodes for electrical double layer capacitor. *J Energy Storage*. 2020;32:101798.
47. Whitley D. A genetic algorithm tutorial. *Stat Comput*. 1994;4(2):65-85.
48. Rani MU, Naresh V, Damodar D, Muduli S, Martha SK, Deshpande AS. In-situ formation of mesoporous SnO₂@C nanocomposite electrode for supercapacitors. *Electrochim Acta*. 2021;365:137284.
49. Fuertes AB, Sevilla M. High-surface area carbons from renewable sources with a bimodal micro-mesoporosity for high-performance ionic liquid-based supercapacitors. *Carbon*. 2015;94:41-52.
50. Yan Y, Cheng Q, Zhu Z, Pavlinek V, Saha P, Li C. Controlled synthesis of hierarchical polyaniline nanowires/ordered bimodal mesoporous carbon nanocomposites with high surface area for supercapacitor electrodes. *J Power Sources*. 2013;240:544-550.
51. Kilic MS, Bazant MZ, Ajdari A. Steric effects in the dynamics of electrolytes at large applied voltages. I. Double-layer charging. *Phys Rev E Stat Nonlin Soft Matter Phys*. 2007;75(2):021502.
52. Kilic MS, Bazant MZ, Ajdari A. Steric effects in the dynamics of electrolytes at large applied voltages. II. Modified Poisson-Nernst-Planck equations. *Phys Rev E Stat Nonlin Soft Matter Phys*. 2007;75(2):021503.
53. Ge R, Boyce AM, Shui Zhang Y, Shearing PR, Cumming DJ, Smith RM. Discrete element method and electrochemical modelling of lithium ion cathode structures characterised by X-ray computed tomography. *Chem Eng J*. 2023;465:142749.
54. Harris AB, Fisch R. Critical behavior of random resistor networks. *Phys Rev Lett*. 1977;38(15):796-799.
55. Xu X, Wang J, Lv JP, Deng Y. Simultaneous analysis of three-dimensional percolation models. *Front Phys*. 2014;9(1):113-119.
56. Arand F, Hesser J. Accurate and efficient maximal ball algorithm for pore network extraction. *Comput Geosci*. 2017;101:28-37.

SUPPORTING INFORMATION

Additional supporting information can be found online in the Supporting Information section at the end of this article.

How to cite this article: Huang P, Tao H, Liu H, Lian C. Accelerating charging dynamics using self-driven optimizing porous structures. *AIChE J*. 2024;70(4):e18313. doi:[10.1002/aic.18313](https://doi.org/10.1002/aic.18313)